Electronic Supplementary Material (ESI) for Physical Chemistry Chemical Physics

Resonant X-Ray Emission Spectroscopy Reveals d–d Ligand-Field States Involved in the Self-Assembly of a Square-Planar Platinum Complex

Claudio Garino, Erik Gallo, Nikolay Smolentsev, Pieter Glatzel, Roberto Gobetto, Carlo Lamberti, Peter J. Sadler and Luca Salassa

Supporting Information

Table of Contents

Experimental section 2
Materials and methods 2
Sample preparation 2
Data acquisition 2
Data analysis 2
Computational details 2
Results 4
Figure SI1 4
Figure SI2 5
Figure SI3 6
Figure SI4 7
Table SI1 8
Figure SI5 10
Figure SI6 11
References 12

Experimental section

Materials and methods. $K_2[PtCl_4]$ was obtained from Precious Metals Online, 2,2';6',2''-terpyridine (tpy) was obtained from Sigma-Aldrich. All solvents were purchased from Carlo Erba.

Sample preparation. The complex [Pt(tpy)(Cl)]Cl was synthetized using literature methods and characterized accordingly.[1] ^{1}H NMR, ^{13}C NMR, and UV-Vis successfully confirmed the structure of the product obtained. Four aqueous solutions (40, 20, 10, 5 mM) and a pellet of [Pt(tpy)(Cl)]Cl were prepared for X-ray measurements. $K_2[PtCl_4]$ (reference) was measured as pellet.

Data acquisition. RXES measurements were performed on the high brilliance X-ray spectroscopy beamline ID26 at the European Synchrotron Radiation Facility (ESRF). The electron energy was 6.0 GeV with a ring current between 170 mA and 200 mA. The incident energy was selected by using the <311> reflection of a pair of cryogenically cooled Si single crystals. Higher harmonics were suppressed using two mirrors with a Pd/Cr coating operating in total reflection at 2.5 mrad. The total flux on the samples was about $5 \cdot 10^{12}$ photon s^{-1}. The beam size was approximately 0.8 mm horizontal and 0.2 mm vertical. The emitted X-rays were analyzed using a spectrometer in vertical Rowland geometry equipped with a spherically bent (R = 1 m, diameter = 50 mm) single crystal wafer in Si <933> Bragg reflection. The selected photons were detected by means of an avalanche photodiode (APD) with an active area of 10 x 10 mm^2 and a thickness of the Si layer of 200 µm. The combined energy bandwidth (incident convoluted with the emission energy bandwidth) was about 1.5 eV. The sample was measured at room temperature and no radiation damage was observed as monitored by fast (5 s) XANES scans measured using a photodiode.

Data analysis. The spectral intensity in RXES map was normalized to unity in the maximum of the main peak arising in the region between 4 and 6 eV. We analyzed the spectral features of the RXES maps using a first moment analysis after removing intensity arising from the elastic peak at 0 eV energy transfer (see Figure SI6). Denoting the energies and fluorescence intensities as *Ej* and *Ij*, respectively, of the j^{th} data point, all data points with intensities greater than *p (= 0.2)* percent of the maximum intensity are included in the calculation of $M1^P$:

$$M1^P = \frac{\sum_j^n E_j I_j}{\sum_j^n I_j}$$

The details of the use of the first moment analysis can be found elsewhere.[2]

Computational details. RXES maps were simulated using the dipole transition matrix elements obtained with a simplified version of the Kramers-Heisenberg equation.[3] that gives the Resonant X-ray emission spectra in the single electron transition approximation:

$$\frac{d\sigma_{resonant}(\varpi_1,\varpi_2)}{d\Omega} \propto \int_{\varepsilon} \frac{\rho(\varepsilon)M(\varepsilon)\rho'(\varepsilon+\omega_1-\omega_2)M(\varepsilon+\omega_1-\omega_2)}{(\varepsilon-\omega_2)^2+\frac{\Gamma_n^2}{4}} d\varepsilon$$

where $d\sigma/d\Omega$ is the differential cross-section and ω_1 and ω_2 are the incident and emitted photon energies, respectively, and Γ_n is the life time (in full width at half maximum) of the intermediate states. Occupied density of states is given as $\rho(\varepsilon)$ and unoccupied as $\rho'(\varepsilon)$, $M(\varepsilon)$ is the radial transition probability.
An elastic peak due to Thomson scattering was added to the RXES planes to facilitate comparison with experiment. The following value was used for the lifetime broadening of the $2p_{3/2}$ core hole: 5.31 eV.[4] All calculated RXES maps were convoluted with additional Gaussian broadening of 1.2 eV for emitted energy and 0.3 eV for incident energy.

The electronic structures (in particular the angular momentum projected DOS) used for the map simulations were obtained within the DFT framework with the full-potential self-consistent WIEN2k code,[5] adopting the generalized gradient approximation form derived by Perdew et al.[6] as exchange-correlation potential. As input geometries, the X-ray structures published by Bailey et al.[7] and by Dickinson[8] were employed in the case of [Pt(tpy)Cl]Cl (head-to-tail dimer in unit cell) and $K_2[PtCl_4]$ respectively. The basis functions for the valence orbitals were expanded simultaneously as spherical harmonics (inside non-overlapping atomic spheres centered at the atomic sites) and as plane waves in the interstitial region. The plane waves were expanded up to a cut-off parameter, k_{max}, fulfilling the relation $R_A k_{max} = 7$ where R_A is the radius of the smallest atomic sphere. We used automatically selected values of atomic radii. The energy separation value between valence and core orbitals was set to 82 eV for all compounds. The self-consistent iteration process was repeated until an energy convergence of $1.3 \cdot 10^{-3}$ eV was reached. The number of k points in the Brillion zone was set to N = 500 as a compromise between precision and computational time. We have performed convergence test for Rk_{max} up to 9 and for N up to 5000 and we have found negligible changes in the RXES maps.

Geometry optimization of $[Pt(tpy)(Cl)]^+$, in the singlet ground state, was performed with the Gaussian 09 program package (revision A.2),[9] employing the DFT method. The nature of the stationary point was confirmed by normal-mode analysis. A total of 64 singlet excited states were determined with a TDDFT[10] calculation. The conductor-like polarizable continuum model (CPCM)[11] with water as the solvent was used to calculate the geometry, the electronic structure, and the electronic excited states in solution. After testing four different functionals (BP86,[12] B3LYP,[13] PBE1PBE,[14] and TPSSH[15]), the TPSSH functional was chosen, together with the SDD basis set[16] and effective core potential for the Pt atom, and the 6-31+G** basis set[17] for all the other atoms. Electronic structure calculation for head-to-tail oligomeric aggregates $\{[Pt(tpy)Cl]^+\}_n$ (where n = 2, 4, 6, 8, 10) were evaluated in gas phase, at the TPSSH/SDD/6-31+G** level. The structures for theoretical calculations were constructed employing the X-ray data available for $[Pt(tpy)Cl]ClO_4$.[7] The complex crystallizes in the monoclinic $P2_1/c$ space group and the cations form a continuous stack along the axial direction, with alternating short/long Pt-Pt distances (3.269 and 4.197 Å, respectively). Six oligomers were obtained stacking 2, 4, 6, 8, and 10 cations along the axial direction, as reported in Figure SI4. The program GaussSum 2.2.4[18] was used to simulate the electronic spectra and to visualize the excited state transitions as electron density difference maps (EDDMs).[19]

Results

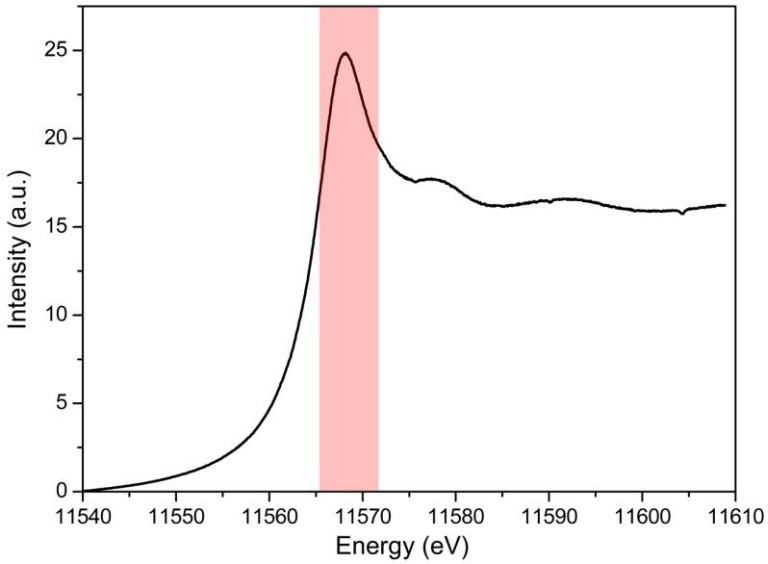

Figure SI1. Pt-L_3 Total Fluorescent Yield (TFY) XANES spectrum of [Pt(tpy)(Cl)]Cl in the solid state. The "red" box highlights the incident energy region where the Valence-to-Core Pt-L_3($2p_{3/2}$) RXES map was collected.

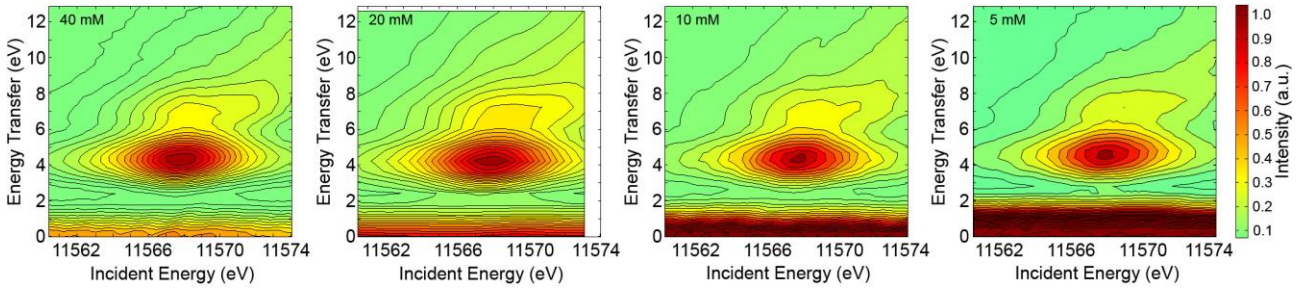

Figure SI2. Experimental Pt-L_3 ($2p_{3/2}$) RXES planes obtained by measurements on aqueous solution of [Pt(tpy)Cl]Cl at different concentrations (5, 10, 20, and 40 mM).

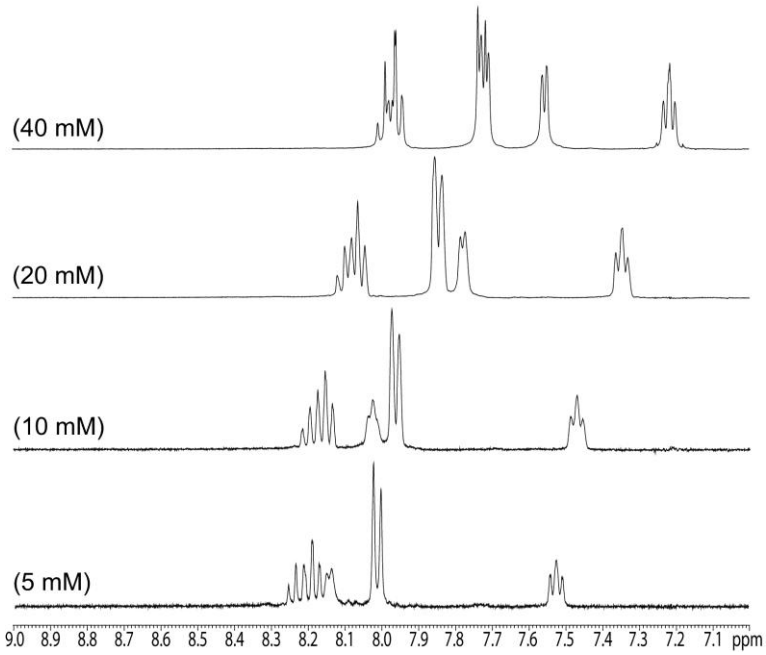

Figure SI3. ^{1}H NMR spectra of [Pt(tpy)(Cl)]Cl in D_2O at different concentrations (40, 20, 10, 5 mM).

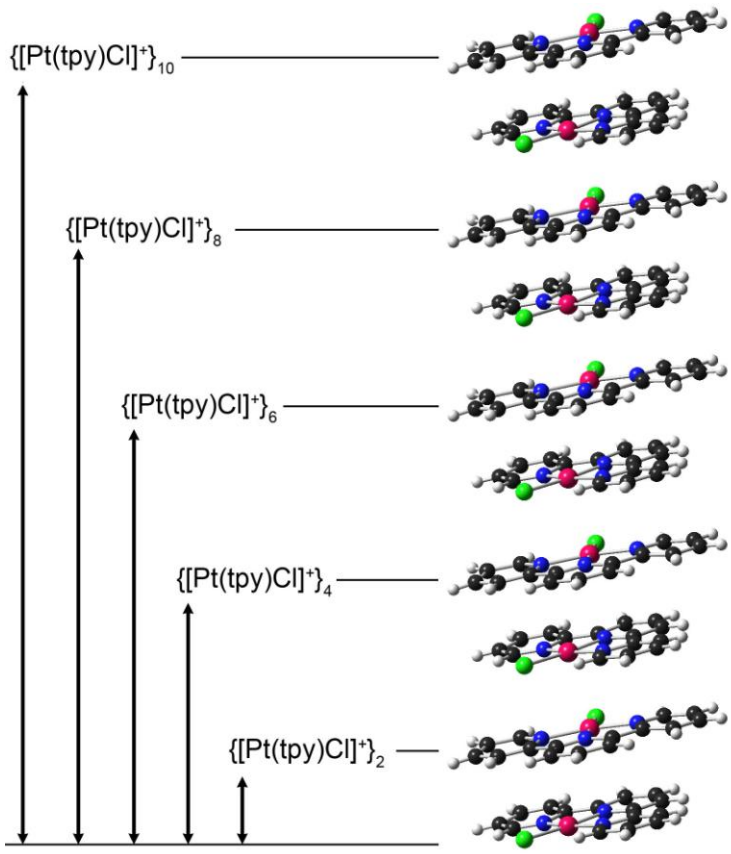

Figure SI4. Structures of head-to-tail oligomeric aggregates $\{[Pt(tpy)Cl]^{+}\}_{n}$ (where n = 2, 4, 6, 8, 10) employed in theoretical calculations.

Table SI1. Calculated Singlet Excited-States Transitions for $[Pt(tpy)(Cl)]^+$ in Water.

Tr.[a]	Energy (eV)	*f*[b]	Major contributions	Minor contributions
1	2.77	0.0041	H-1→LUMO (100%)	
2	2.99	0.0369	HOMO→LUMO (94%)	H-2→L+1 (3%)
3	3.07	0.0018	H-2→LUMO (99%)	
4	3.22	0.0	H-3→LUMO (96%)	H-1→L+1 (4%)
5	3.27	0.0006	H-1→L+1 (90%)	H-3→LUMO (3%), HOMO→L+1 (6%)
6	3.27	0.0093	HOMO→L+1 (89%)	H-4→LUMO (5%), H-1→L+1 (6%)
7	3.69	0.0514	H-4→L+1 (10%), H-2→L+1 (79%)	H-1→L+3 (3%), HOMO→LUMO (3%)
8	3.70	0.0002	H-3→L+1 (98%)	
9	3.73	0.3371	H-4→LUMO (88%)	H-2→L+2 (4%), HOMO→L+1 (4%)
10	3.95	0.0003	H-1→L+3 (93%)	H-5→LUMO (2%), H-2→L+1 (2%)
11	4.02	0.0	HOMO→L+3 (97%)	
12	4.21	0.0027	H-4→L+1 (26%), HOMO→L+2 (67%)	H-2→L+4 (3%)
13	4.22	0.0008	H-1→L+2 (99%)	
14	4.24	0.0	H-2→L+3 (47%), H-1→L+4 (48%)	H-4→L+3 (3%)
15	4.27	0.0622	H-5→LUMO (13%), H-4→L+1 (43%), HOMO→L+2 (27%)	H-6→LUMO (7%), H-2→L+1 (6%)
16	4.28	0.0001	HOMO→L+4 (91%)	H-3→L+3 (8%)
17	4.31	0.0009	H-2→L+3 (41%), H-1→L+4 (48%)	H-7→LUMO (2%), H-3→L+3 (6%)
18	4.31	0.0118	H-3→L+3 (81%)	H-7→L+3 (2%), H-2→L+3 (3%), H-1→L+4 (3%), HOMO→L+4 (7%)
19	4.41	0.0392	H-6→LUMO (17%), H-5→LUMO (67%)	H-4→L+1 (2%), H-2→L+4 (6%), H-1→L+3 (3%)
20	4.56	0.1437	H-5→L+1 (25%), H-2→L+2 (71%)	H-4→LUMO (2%)
21	4.62	0.0	H-3→L+2 (99%)	
22	4.64	0.1102	H-6→LUMO (60%), H-2→L+4 (17%)	H-8→LUMO (2%), H-5→LUMO (3%), H-4→L+1 (2%), H-2→L+1 (3%), HOMO→L+2 (2%), HOMO→L+5 (8%)
23	4.70	0.0001	H-3→L+4 (99%)	
24	4.76	0.0501	H-8→LUMO (11%), H-2→L+4 (56%)	H-6→LUMO (7%), H-5→LUMO (9%), H-4→L+1 (9%), H-4→L+4 (2%), HOMO→L+5 (2%)
25	4.77	0.0	H-7→LUMO (91%)	H-4→L+3 (3%), H-2→L+3 (4%)
26	4.83	0.5354	H-5→L+1 (66%), H-2→L+2 (20%)	H-6→L+1 (7%), H-4→LUMO (3%)
27	4.87	0.0	H-4→L+3 (92%)	H-7→LUMO (5%), H-2→L+3 (3%)
28	4.95	0.0634	H-6→L+1 (84%)	H-11→LUMO (2%), H-5→L+1 (5%), H-4→L+2 (3%), H-2→L+5 (3%)
29	4.96	0.0003	H-9→LUMO (98%)	
30	5.05	0.0001	H-1→L+5 (99%)	
31	5.08	0.002	H-4→L+2 (86%)	H-10→LUMO (3%), H-8→L+1 (2%), H-6→L+1 (2%), H-2→L+5 (4%)
32	5.17	0.1077	H-8→LUMO (14%), H-4→L+4 (50%), HOMO→L+5 (20%)	H-8→L+2 (2%), H-6→LUMO (2%), H-5→LUMO (2%), H-4→L+1 (2%), H-2→L+4 (4%)
33	5.18	0.1024	H-8→LUMO (17%), HOMO→L+5 (62%)	H-6→LUMO (3%), H-4→L+4 (8%), H-2→L+4 (3%), H-1→L+7 (2%)
34	5.22	0.0	H-7→L+1 (99%)	
35	5.24	0.0015	H-8→LUMO (46%), H-4→L+4 (32%)	H-10→L+1 (2%), H-5→L+2 (8%), H-2→L+4 (4%), HOMO→L+5 (4%)
36	5.32	0.0098	H-11→LUMO (12%), H-10→LUMO (11%), H-2→L+5 (72%)	
37	5.42	0.0	H-9→L+1 (99%)	
38	5.47	0.0156	H-11→LUMO (22%), H-10→LUMO (39%), H-8→L+1 (37%)	
39	5.48	0.0	H-3→L+5 (99%)	
40	5.52	0.0	H-5→L+3 (95%)	H-6→L+3 (5%)
41	5.53	0.0007	H-10→LUMO (19%), H-8→L+1 (41%), H-5→L+4 (31%)	H-11→LUMO (4%)
42	5.61	0.003	H-11→LUMO (39%), H-4→L+5 (27%)	H-10→LUMO (6%), H-8→L+1 (4%),

				H-5→L+4 (8%), H-2→L+5 (6%), HOMO→L+6 (4%)
43	5.68	0.0132	H-12→LUMO (50%), H-6→L+2 (10%), H-5→L+2 (30%)	H-10→L+1 (3%)
44	5.73	0.0	H-6→L+3 (93%)	H-5→L+3 (5%)
45	5.75	0.0261	H-12→LUMO (37%), H-11→L+1 (14%), H-5→L+2 (36%)	H-10→L+1 (3%), H-6→L+2 (6%)
46	5.76	0.0	H-13→LUMO (99%)	
47	5.80	0.0107	H-12→L+1 (18%), H-4→L+5 (37%), HOMO→L+6 (19%)	H-11→LUMO (6%), H-10→LUMO (4%), H-5→L+4 (7%), H-2→L+5 (4%)
48	5.85	0.0489	H-6→L+4 (60%), H-5→L+4 (18%)	H-10→LUMO (3%), H-8→L+1 (2%), H-7→L+3 (7%), H-4→L+5 (7%)
49	5.88	0.015	H-10→L+1 (35%), H-6→L+2 (58%)	H-11→L+1 (2%)
50	5.91	0.0715	H-7→L+3 (81%)	H-13→L+3 (5%), H-6→L+4 (8%), H-3→L+3 (2%)
51	5.93	0.0	H-1→L+6 (100%)	
52	5.96	0.0034	H-12→L+1 (21%), HOMO→L+6 (65%)	H-11→LUMO (2%), H-10→LUMO (2%), H-6→L+4 (4%)
53	5.96	0.0112	HOMO→L+7 (99%)	
54	6.00	0.0203	H-11→L+1 (22%), H-10→L+1 (27%), H-2→L+6 (33%)	H-12→LUMO (2%), H-6→L+2 (9%), H-1→L+7 (2%)
55	6.11	0.0489	H-11→L+1 (20%), H-1→L+7 (59%)	H-6→L+2 (2%), H-6→L+5 (2%), H-5→L+2 (5%), H-4→L+6 (6%)
56	6.13	0.0	H-7→L+2 (99%)	
57	6.14	0.0408	H-11→L+1 (25%), H-10→L+1 (10%), H-1→L+7 (32%)	H-12→LUMO (2%), H-6→L+2 (7%), H-5→L+2 (8%), H-4→L+6 (5%)
58	6.19	0.0	H-13→L+1 (24%), H-7→L+4 (67%)	H-14→LUMO (4%), H-8→L+3 (2%)
59	6.20	0.0-	H-13→L+1 (64%), H-7→L+4 (30%)	H-14→LUMO (4%)
60	6.24	0.1642	H-6→L+4 (23%), H-5→L+4 (25%), H-4→L+5 (16%)	H-11→LUMO (3%), H-11→L+2 (6%), H-10→LUMO (3%), H-10→L+2 (4%), H-8→L+1 (7%), H-4→L+2 (2%), HOMO→L+6 (4%)
61	6.27	0.0	H-2→L+7 (98%)	
62	6.35	0.0001	H-8→L+3 (89%)	H-13→L+1 (2%), H-3→L+6 (7%)
63	6.36	0.0	H-9→L+2 (10%), H-3→L+6 (83%)	H-8→L+3 (5%)
64	6.36	0.0	H-9→L+2 (86%)	H-8→L+3 (3%), H-3→L+6 (9%)

[a] Tr. indicates transition number as obtained in the TDDFT calculation output. [b] *f* = oscillator strength.

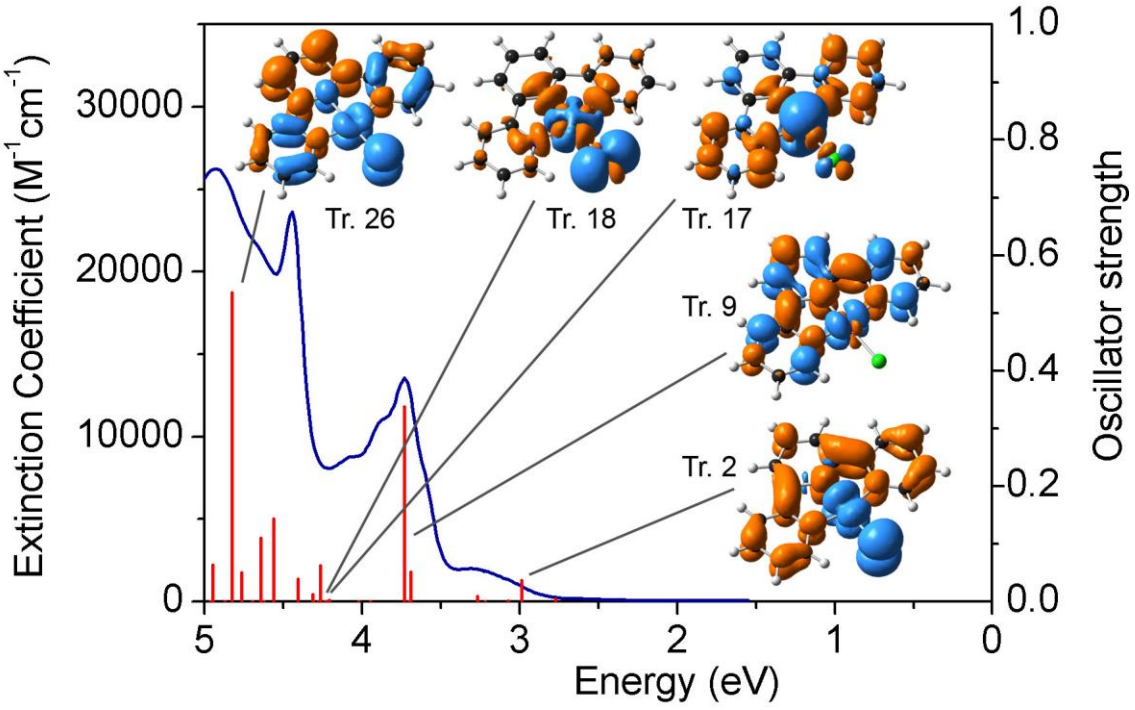

Figure SI5. Experimental UV-Vis absorption spectrum for an aqueous solution of [Pt(tpy)Cl]Cl (blue line) and calculated singlet excited state transitions (red bars). EDDMs electron-density difference maps) of the foremost electronic transitions are also shown (blue indicates a decrease in electron density, orange indicates an increase; isovalue = 0.001).

In aqueous solution the spectrum shows two intense absorption bands in the range 5–4 eV (250–300 nm) and a lower intensity band at 4–3.5 eV (300–350 nm) with a tail at 3.3 eV, which extends into the visible region. TDDFT singlet calculations (Table SI1) on the monomeric complex assign the high-energy absorption bands (5–4 eV) to mixed π–π*/MLCT electronic transitions (π–π* = tpy, MLCT = Pt,Cl → tpy). The feature at 4–3.5 eV has a π–π* (tpy) character, while the tail at 3.3 eV can be ascribed to MLCT transitions (Pt,Cl → tpy). The electron density differences maps (EDDMs) reported give pictorial representations of such assignment. Weak d–d LF transitions are placed by TDDFT at the 5–4 eV (EDDMs S17 and S18). These involve the Pt(d)-containing LUMO+3 and HOMO–2 and HOMO–3 orbitals and have low oscillator strength probability.

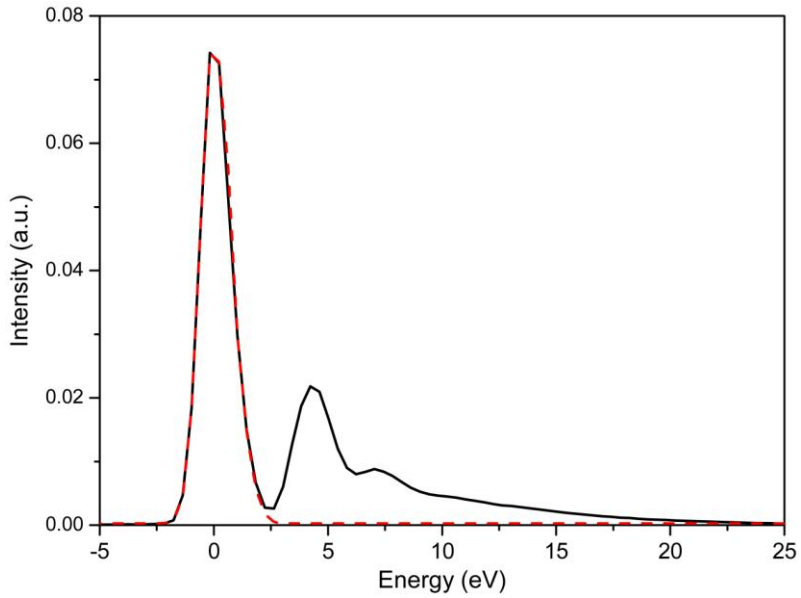

Figure SI6. Fit (dashed red line) of the elastic peak in the CIE cut at 11567 eV (black line) of the Pt-L_3 ($2p_{3/2}$) RXES plane for [Pt(tpy)Cl]Cl (10mM aqueous solutions).

References

[1] M. Howe-Grant, S. J. Lippard, P. Chalilpoyil, L. G. Marzilli, in *Inorg. Synth.*, John Wiley & Sons, Inc., **1980**, pp. 101-105.
[2] P. Glatzel, U. Bergmann, J. Yano, H. Visser, J. H. Robblee, W. W. Gu, F. M. F. de Groot, G. Christou, V. L. Pecoraro, S. P. Cramer, V. K. Yachandra, *J. Am. Chem. Soc.* **2004**, *126*, 9946-9959; E. Gallo, C. Lamberti, P. Glatzel, *Phys. Chem. Chem. Phys.* **2011**, *13*, 19409-19419.
[3] J. Jimenez-Mier, J. van Ek, D. L. Ederer, T. A. Callcott, J. J. Jia, J. Carlisle, L. Terminello, A. Asfaw, R. C. Perera, *Phys. Rev. B* **1999**, *59*, 2649-2658; P. Glatzel, J. Singh, K. O. Kvashnina, J. A. van Bokhoven, *J. Am. Chem. Soc.* **2010**, *132*, 2555-2557; N. Smolentsev, M. Sikora, A. V. Soldatov, K. O. Kvashnina, P. Glatzel, *Phys. Rev. B* **2011**, *84*.
[4] J. C. Fuggle, J. E. Inglesfield, *Top. Appl. Phys.* **1992**, *69*, 1-23.
[5] P. Blaha, K. Schwarz, G. K. H. Madsen, D. Kvasnicka, J. Luitz, Karlheinz Schwarz Technische Universität, Wien, Austria, **2001**; K. Schwarz, P. Blaha, S. B. Trickey, *Mol. Phys.* **2010**, *108*, 3147-3166.
[6] J. P. Perdew, K. Burke, M. Ernzerhof, *Phys. Rev. Lett.* **1996**, *77*, 3865-3868.
[7] J. A. Bailey, M. G. Hill, R. E. Marsh, V. M. Miskowski, W. P. Schaefer, H. B. Gray, *Inorg. Chem.* **1995**, *34*, 4591-4599.
[8] R. G. Dickinson, *J. Am. Chem. Soc.* **1922**, *44*, 2404-2411.
[9] M. J. Frisch, G. W. Trucks, H. B. Schlegel, G. E. Scuseria, M. A. Robb, J. R. Cheeseman, G. Scalmani, V. Barone, B. Mennucci, G. A. Petersson, H. Nakatsuji, M. Caricato, X. Li, H. P. Hratchian, A. F. Izmaylov, J. Bloino, G. Zheng, J. L. Sonnenberg, M. Hada, M. Ehara, K. Toyota, R. Fukuda, J. Hasegawa, M. Ishida, T. Nakajima, Y. Honda, O. Kitao, H. Nakai, T. Vreven, J. Montgomery, J. A., J. E. Peralta, F. Ogliaro, M. Bearpark, J. J. Heyd, E. Brothers, K. N. Kudin, V. N. Staroverov, R. Kobayashi, J. Normand, K. Raghavachari, A. Rendell, J. C. Burant, S. S. Iyengar, J. Tomasi, M. Cossi, N. Rega, N. J. Millam, M. Klene, J. E. Knox, J. B. Cross, V. Bakken, C. Adamo, J. Jaramillo, R. Gomperts, R. E. Stratmann, O. Yazyev, A. J. Austin, R. Cammi, C. Pomelli, J. W. Ochterski, R. L. Martin, K. Morokuma, V. G. Zakrzewski, G. A. Voth, P. Salvador, J. J. Dannenberg, S. Dapprich, A. D. Daniels, Ö. Farkas, J. B. Foresman, J. V. Ortiz, J. Cioslowski, D. J. Fox, Revision A.1 ed., Gaussian, Inc., Wallingford, CT, **2009**.
[10] A. Vlček, S. Záliš, *Coord. Chem. Rev.* **2007**, *251*, 258-287.
[11] M. Cossi, N. Rega, G. Scalmani, V. Barone, *J. Comput. Chem.* **2003**, *24*, 669-681.
[12] A. D. Becke, *Phys. Rev. A* **1988**, *38*, 3098-3100; J. P. Perdew, *Phys. Rev. B* **1986**, *33*, 8822-8824.
[13] A. D. Becke, *J. Chem. Phys.* **1993**, *98*, 5648-5652; C. T. Lee, W. T. Yang, R. G. Parr, *Phys. Rev. B* **1988**, *37*, 785-789.
[14] J. P. Perdew, K. Burke, M. Ernzerhof, *Phys. Rev. Lett.* **1997**, *78*, 1396-1396; C. Adamo, G. E. Scuseria, V. Barone, *J. Chem. Phys.* **1999**, *111*, 2889-2899.
[15] J. Tao, J. P. Perdew, V. N. Staroverov, G. E. Scuseria, *Phys. Rev. Lett.* **2003**, *91*, 146401.
[16] P. Fuentealba, H. Preuss, H. Stoll, L. Von Szentpály, *Chem. Phys. Lett.* **1982**, *89*, 418-422.
[17] R. Ditchfield, W. J. Hehre, J. A. Pople, *J. Chem. Phys.* **1971**, *54*, 724-728.
[18] N. M. O'Boyle, A. L. Tenderholt, K. M. Langner, *J. Comput. Chem.* **2008**, *29*, 839-845.
[19] M. Head-Gordon, A. M. Grana, D. Maurice, C. A. White, *J. Phys. Chem.* **1995**, *99*, 14261-14270; W. R. Browne, N. M. O'Boyle, J. J. McGarvey, J. G. Vos, *Chem. Soc. Rev.* **2005**, *34*, 641-663.